

Influence of Tetraethoxysilane Addition in Siloxane-Poly(Methyl Methacrylate) Hybrid Films Applied on Galvanized Steel

Sandra Raquel Kunst^{1,}, Henrique Ribeiro Piaggio Cardoso¹, Cláudia Trindade Oliveira², Cícero Inácio da Silva Filho³, Victor Hugo Vitorino Sarmiento³, Tiago Lemos Menezes⁴, Iduvirges Lourdes Müller¹, Célia de Fraga Malfatti¹.*

¹LAPEC, Federal University of Rio Grande do Sul – UFRGS, Avenida Bento Gonçalves, 9500, Porto Alegre – RS - Brazil.

²ICET, Feevale University, RS-239, 2755, Novo Hamburgo – RS - Brazil.

³Department of Chemistry, Federal University of Sergipe – UFS, Avenida. Vereador Olímpio Grande s/n, Centro, Itabaiana – SE – Brazil.

⁴LACOR, Federal University of Rio Grande do Sul – UFRGS, Avenida Bento Gonçalves, 9500, Porto Alegre – RS - Brazil.

*E-mail: tessaro.sandra@gmail.com

Received: 2 July 2013 / Accepted: 11 August 2013 / Published: 10 September 2013

Hybrid films of siloxane-poly(methyl methacrylate) (PMMA) are used as coatings in materials such as galvanized steel and alloys and have also recently been used as bulk materials. To improve the performance of these films, new formulations have been developed with the introduction of plasticizer agents to improve zinc corrosion resistance and to increase the layer thickness in order to more evenly coat the rough surface of galvanized steel. In this context, the aim of this paper is to coat galvanized steel with a hybrid film of PMMA and a mixture consisting of the alkoxides 3-(trimethoxysilylpropyl) methacrylate (TMSM) and tetraethoxysilane (TEOS). The hybrid films were applied by dip-coating and curing for 3 hours at a temperature of 160 °C. Samples with and without TEOS were characterized by electrochemical impedance spectroscopy (EIS), and the open circuit potential was monitored in a 0.05 M NaCl solution. The hydrophobicity of the film was determined by contact angle measurements. Morphological aspects were evaluated by scanning electron microscopy (SEM) and atomic force microscopy (AFM). FT-IR measurements were recorded to characterize the films. The mechanical behavior was evaluated by tribology trials of attrition. The results obtained for the T4AN01 film showed a higher thickness associated with the presence of TEOS in the film, which increases the silanol content and, consequently, the amount of inorganic phase (siloxane). The EIS results showed that the T4AN01 coating displayed the best performance.

Keywords: Galvanized steel; Hybrid films; TEOS; EIS; Corrosion.

1. INTRODUCTION

Hybrid films of different chemical formulation are currently used for the pre-treatment of different metallic substrates, such as galvanized steel, steel, aluminum and its alloys, copper, and magnesium [1-14]. In particular, hybrid sol-gel-derived materials are very versatile, combining the complementary properties of the inorganic and organic materials that constitute them [15-21]. The current availability of a large number of precursors for the inorganic component, such as metal alkoxides, organo(alkoxy)silanes, and nanoparticles, and their compatibility with polymerizable groups such as methacryloxy, vinyl, and epoxy groups, makes it possible to obtain a wide variety of hybrid sol-gel-derived materials [22-29]. These types of materials are mainly used as coatings for different purposes and have also recently been used as bulk materials. They consist of a dual polymer network, in which cluster- or polymer-type inorganic structures are linked to organic groups or polymer fragments [15,16-24].

New materials from PMMA, as polymeric blends [30,31] and organic-inorganic hybrid materials, have been investigated with the intention of optimizing their properties. These materials are classified according to their chemical bond characteristics and can be conveniently divided into two general classes. Class I corresponds to hybrid films, where organic molecules, oligomers, or low-molecular-weight organic polymers are simply embedded in an inorganic matrix. Both components, organic and inorganic, exchange rather weak bonds, mainly through Van der Waals, hydrogen, or ionic interactions. Class II corresponds to hybrid organic-inorganic compounds, where the organic and inorganic components are bonded through stronger covalent or ionic covalent chemical bonds [16, 18, 19].

Novel and multi-purpose hybrid materials can be obtained by the appropriate choice of inorganic and organic components and their composition [18], for example, to obtain new materials from PMMA. A major challenge in preparing these composite materials is to provide the link between the organic and inorganic phases. The properties of hybrids can be improved by forming covalent bonds between the phases. Thus, the strategy used for researchers is to employ a coupling agent such as a trialkoxysilane functionalized with vinylic ligands, which allows a connection to be made between organic and inorganic phases [32-34]. One widely used trialkoxysilane is 3-methacryloxypropyltrimethoxysilane (TMSM, also known as MPTS). TMSM, besides being a great coupling agent between organic and inorganic phases, is photo-sensitive to UV radiation, which makes it employable in controlling the refractive index, useful in optical devices and in materials with low dielectric constants [35-37]. These characteristics add to the possibility of obtaining coatings some micrometers in thickness without cracks, to the PMMA stability to laser radiation, and to the ease of polymerization of methyl methacrylate (MMA) groups by UV radiation [38] or by heat treatments, allowing the increase of the refractive index.

The present work aims to obtain hybrid films on galvanized steel from poly(methyl methacrylate) (PMMA) and alkoxide precursors: 3-(trimethoxysilylpropyl) methacrylate (TMSM), with and without tetraethoxysilane (TEOS). These films are characterized electrochemically to evaluate their anticorrosion properties.

2. EXPERIMENTAL

2.1. Surface preparation

The galvanized steel substrates ($2 \times 4 \text{ cm}^2$) were degreased with neutral detergent at $70 \text{ }^\circ\text{C}$ by immersion for 10 minutes. After that, the samples were rinsed with deionized water and dried and then rinsed with ethanol and dried. The chemical composition of the samples is listed in Table 1, as provided by the supplier.

Table 1. Galvanized layer composition.

Chemical composition					
Element	C	Mn	S	P	Zn
%wt _{maximum}	0.15	0.6	0.04	0.04	Bal.

2.2. Preparation of the siloxane-PMMA hybrid films

A sol-gel method was employed in the preparation of the hybrid organic-inorganic films. The synthesis of these materials involves three major chemical reactions: hydrolysis of the alkoxide precursors, condensation, leading to the formation of the inorganic phase (polysiloxane), and polymerization of the methacrylate groups. Figure 1 shows the structures of the reagents used in the synthesis of the siloxane-PMMA hybrid nanocomposites.

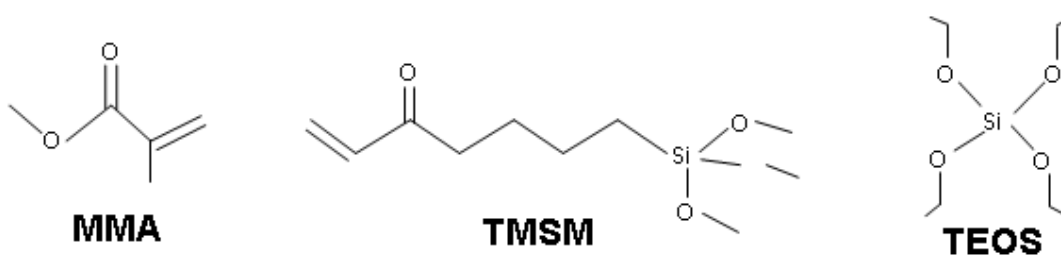


Figure 1. Structural formulas of the reagents used in the synthesis of hybrid films: methyl methacrylate (MMA), 3-methacryloxy-propyl trimethoxy silane (TMSM) and tetraethoxy silane (TEOS).

TMSM is an alkoxide modified by a methacrylate group that acts as a coupling agent between the organic (PMMA) and inorganic (TEOS) components, allowing formation of a class II hybrid material. In the first step of the synthesis, the precursor TEOS, which is responsible for modulating the silicon content in the siloxane phase of the hybrid, was mixed with TMSM at $60 \text{ }^\circ\text{C}$ for 1 hour. The hydrolysis was carried out in acidic medium ($\text{pH}=1$) using HCl as a catalyst and ethanol. Then, the hydrolysis and polycondensation reactions of the alkoxide occurred. Combinations between compounds that present silanol groups ($\text{Si}(\text{OH})_n$) obtained from the hydrolysis of TEOS and TMSM formed siloxane bonds by polycondensation. The second step consisted of homogenization of MMA

and the thermal initiator benzoyl peroxide (BPO) at room temperature. Finally, the two solutions were mixed, forming a homogeneous and transparent solution.

2.3. Application and curing of the siloxane-PMMA hybrid films

The hybrid film deposition on the galvanized steel substrates was performed using dip-coating with a removal rate of 14 cm·min⁻¹. The coated substrates remained in the oven for 24 hours at a temperature of 55 °C. In this step, the polymerization reactions began, promoting the formation of PMMA by radical polyaddition. The hybrid chains were formed from the copolymerization of PMMA with the vinyl group of TMSM, promoted by the radical initiator BPO. Subsequently, the coated substrates were heat treated (cured) at a temperature of 160 °C for 3 hours at a heating rate of 5 °C·min⁻¹. This treatment increases the degree of polymerization because it favors the formation of free radicals from the C=C bonds existing in TMSM and MMA. Table 2 presents the characteristics of the samples, and their preparation protocol is detailed in the flow chart in Figure 2.

Table 2. Description of the samples.

Samples	Description
HDG	Galvanized steel without coating.
T0AN01	Galvanized steel coated with siloxane-PMMA hybrid film without TEOS.
T4AN01	Galvanized steel coated with siloxane-PMMA hybrid film with TEOS.

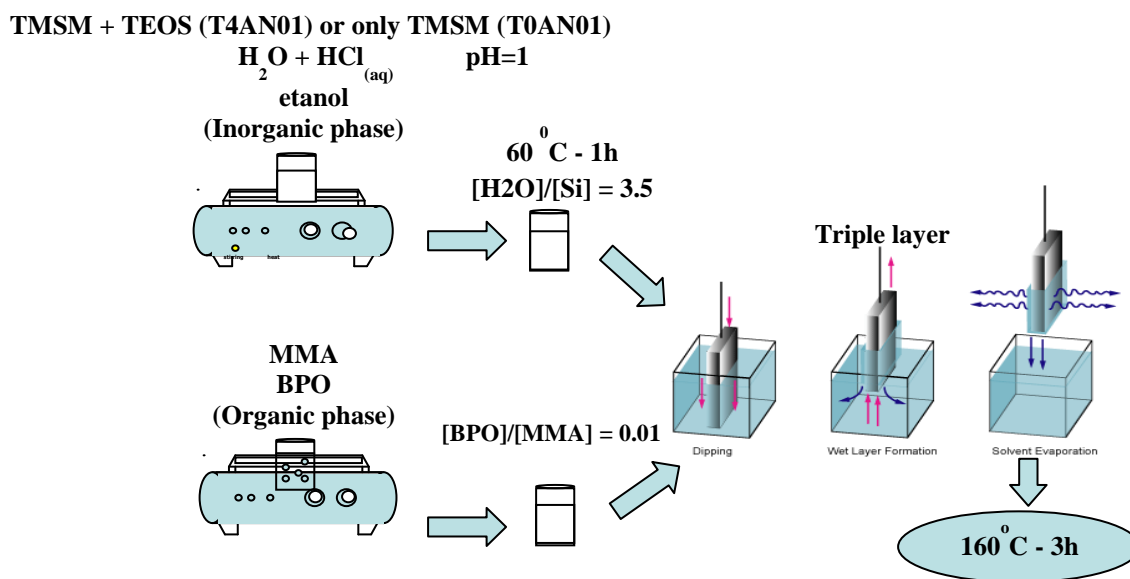


Figure 2. Experimental parameters of synthesis of the sols and processing to deposit coatings.

2.4. Experimental techniques

The morphological characterization was carried out using scanning electron microscopy (SEM), performed with a JEOL 6060 with an acceleration voltage of 20 kV. The samples were observed in top view and cross-section view to determine the layer thickness.

The AFM images were obtained using a SHIMADZU SPM 9600 J3[®] atomic force microscope. AFM images were acquired in dynamic mode to provide information about the topography of the samples.

The wettability of the hybrid films was determined by contact angle measurements using the sessile drop method and home-made equipment. The contact angle was determined using image analysis software.

The infrared spectroscopy measurements were performed on a Spectrum ASCII 100 spectrophotometer. The measurements were performed with the beam in the mid-infrared (2000–500 cm^{-1}). The spectra were obtained from the films without a substrate (free-standing films). For this characterization, two different solutions containing poly(methyl methacrylate) (PMMA) and the alkoxide precursors 3-(trimethoxysilylpropyl) methacrylate (TMSM), with and without tetraethoxysilane (TEOS), were analyzed. The solutions were placed on a petri plate and heated at 55 °C for 24 hours, and cured at 160 °C for 3 hours. After obtaining the film, a small amount of each sample was taken for analysis.

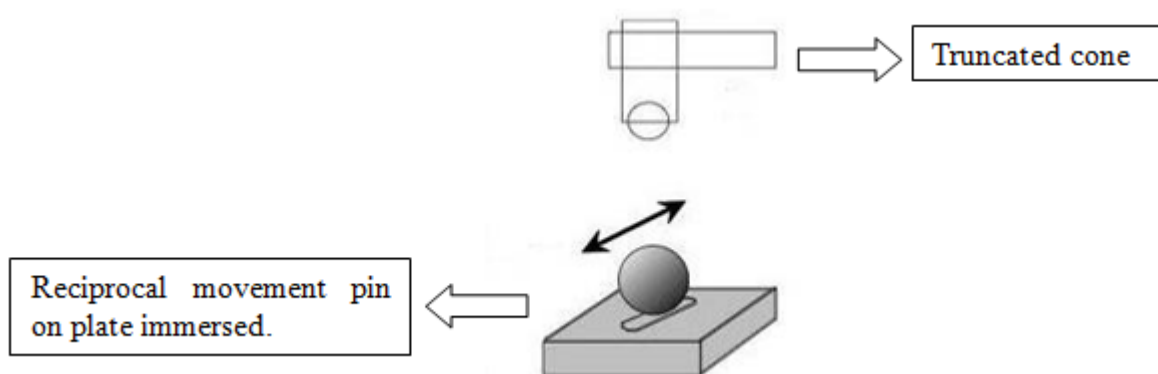


Figure 3. Schematic representation of the tribologic test system.

The corrosion performance of the films was evaluated by open circuit potential (OCP) monitoring, potentiodynamic polarization, and electrochemical impedance spectroscopy (EIS) measurements in a 0.05 M NaCl solution. For the electrochemical experiments, a three-electrode cell was used, with a platinum wire counter electrode and a saturated calomel electrode (SCE) as the reference electrode. The working electrode area was 0.626 cm^2 . OCP monitoring and potentiodynamic polarization were performed with a PAR 273 potentiostat. The OCP was monitored for the first hour of immersion in the electrolyte before the polarization curves and the EIS measurements. The equipment used for the EIS measurements was a potentiostat (Omnimetra Mod. PG-05) coupled to a frequency response analyzer model Solartron 125. The amplitude of the EIS perturbation signal was 10 mV, and the frequency range studied was from 100 kHz to 10 MHz.

The tribologic wear assays were performed with a tribometer, controlled computationally, with the type-setting ball on plate (Figure 3). The wear test was conducted with reciprocal linear movement by a sphere of alumina with a diameter 7.75 mm. We used a constant force of 1.5 N, a frequency of 2 Hz, and a track length of 2 mm.

3. RESULTS AND DISCUSSION

3.1. Morphological characterization

Figures 4 and 5 show the SEM micrographs for the T0AN01 and T4AN01 samples, respectively. The T0AN01 sample (Figure 4) showed small cracks in the coating, while for the T4AN01 sample (Figure 5), the formation of cracks was more accentuated. This must be due to the formation of a completely porous, brittle ceramic structure [39] after hydrolysis and cross-linking of TEOS. In this way, the addition of TEOS contributed to the irregular coverage observed.

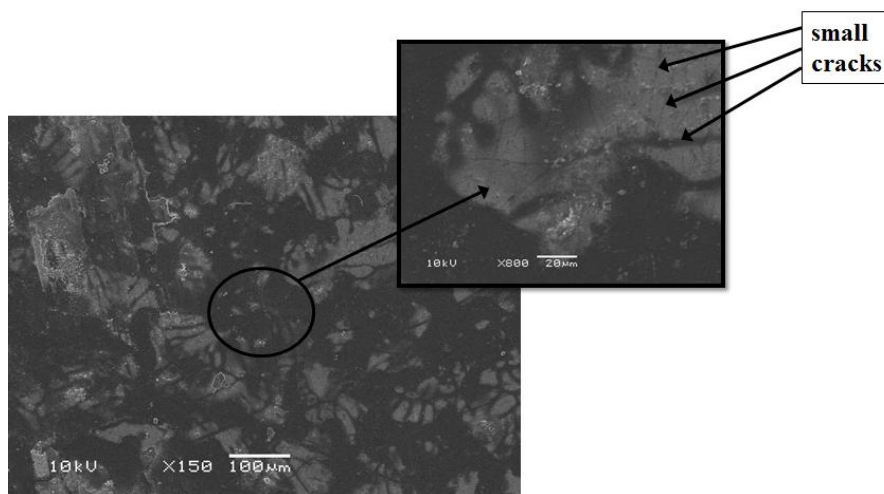


Figure 4. Micrograph obtained by SEM for the T0AN01 film.

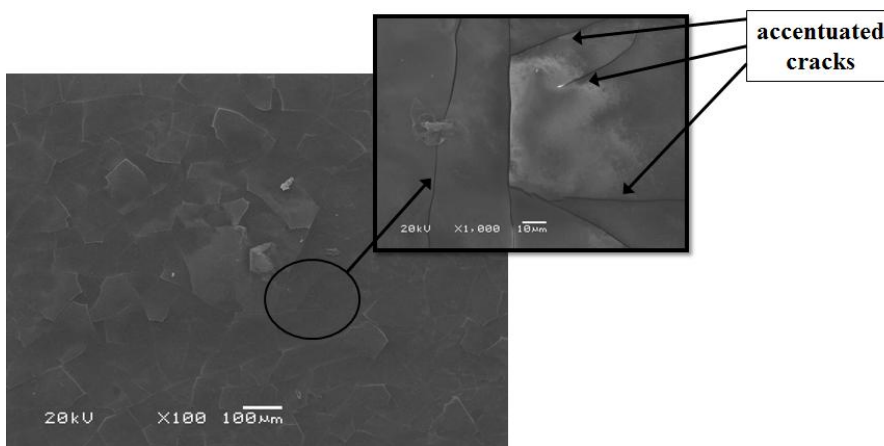


Figure 5. Micrograph obtained by SEM for the T4AN01 film.

Figure 6 shows the images of the cross-sectioned samples with and without TEOS and their EDS analysis. The occurrence of Si in the EDS spectra indicates the presence of the hybrid film, while the Zn in the spectrum is from the galvanized steel substrate. The layer thickness was determined from the cross-section images (Figure 6), and the results are given in Table **Table3**. The film with TEOS (T4AN01) displayed a higher thickness (Figure 6-b). This increased thickness may be related to the fact that the presence of TEOS in the film increases the silanol content and consequently increases the amount of inorganic phase (siloxane). In both hybrid films (T0AN01 and T4AN01), the MMA monomer was mixed with TMSM to increase the compactness of the film structure by polymerization of the acrylate groups and their cross-linking with the silicon network.

The MMA monomer contains only one possible polymerization site per molecule; therefore, during the curing process, each monomer can only have one covalent bond with the TMSM, which, in its turn, has three hydrolyzable groups. Zaioncz et al. [40] reported that the copolymerization of TMSM with MMA monomers gives rise to a cross-linked hybrid compound with the PMMA chains surrounding the siloxane particles. This results in a hybrid structure where the radical MMA covalently bonds to the TMSM moieties through polymerization reactions and can only interact by weak Van der Waals forces [36], which could explain the lower thickness of the hybrid film without TEOS (T0AN01).

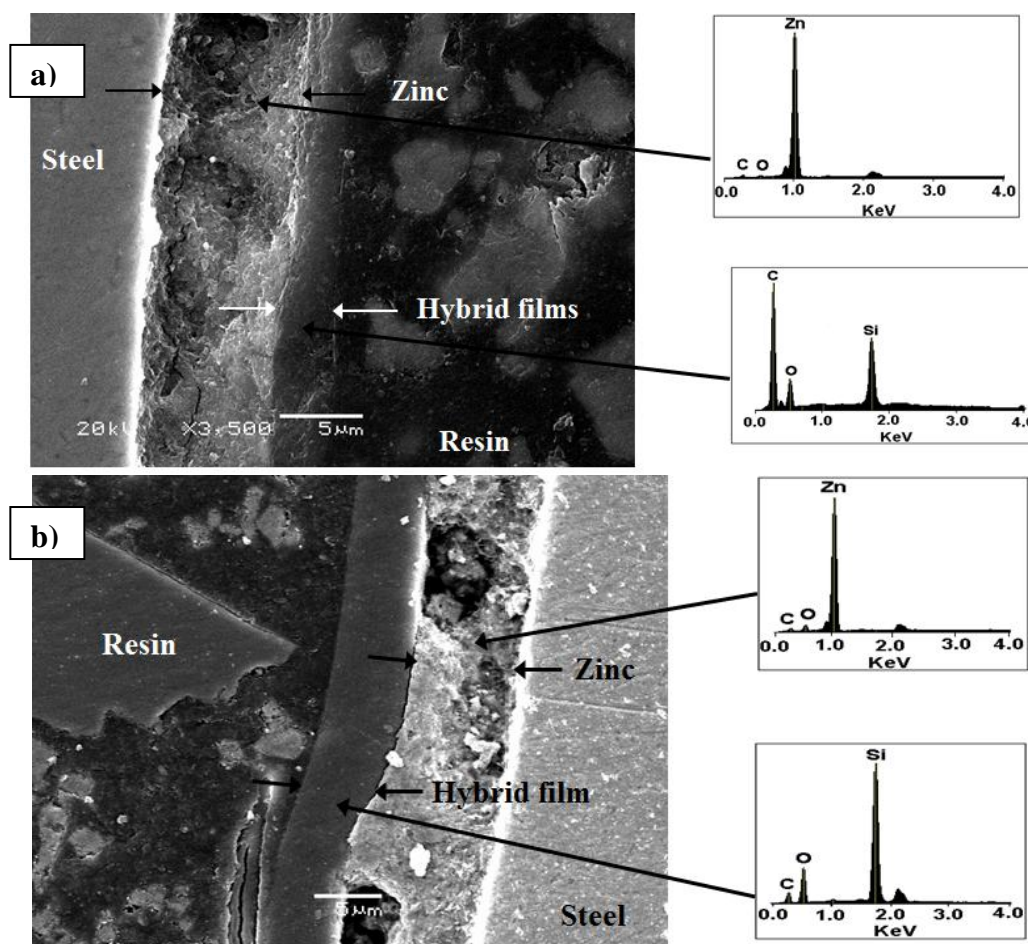


Figure 6. Cross section micrographs obtained by SEM analysis and the corresponding EDS spectrum: (a) T0AN01 and (b) T4AN01.

Table 3. Layer thickness of the hybrid films.

Samples	Thickness (μm)
T0AN01	2.88 ± 0.42
T4AN01	5.12 ± 0.76

Figure 7a–c shows the 3-D AFM images taken from a $70 \times 70 \mu\text{m}^2$ area on the surface of the galvanized steel, T0AN01, and T4AN01, respectively, and the roughness values are shown in Table 3.

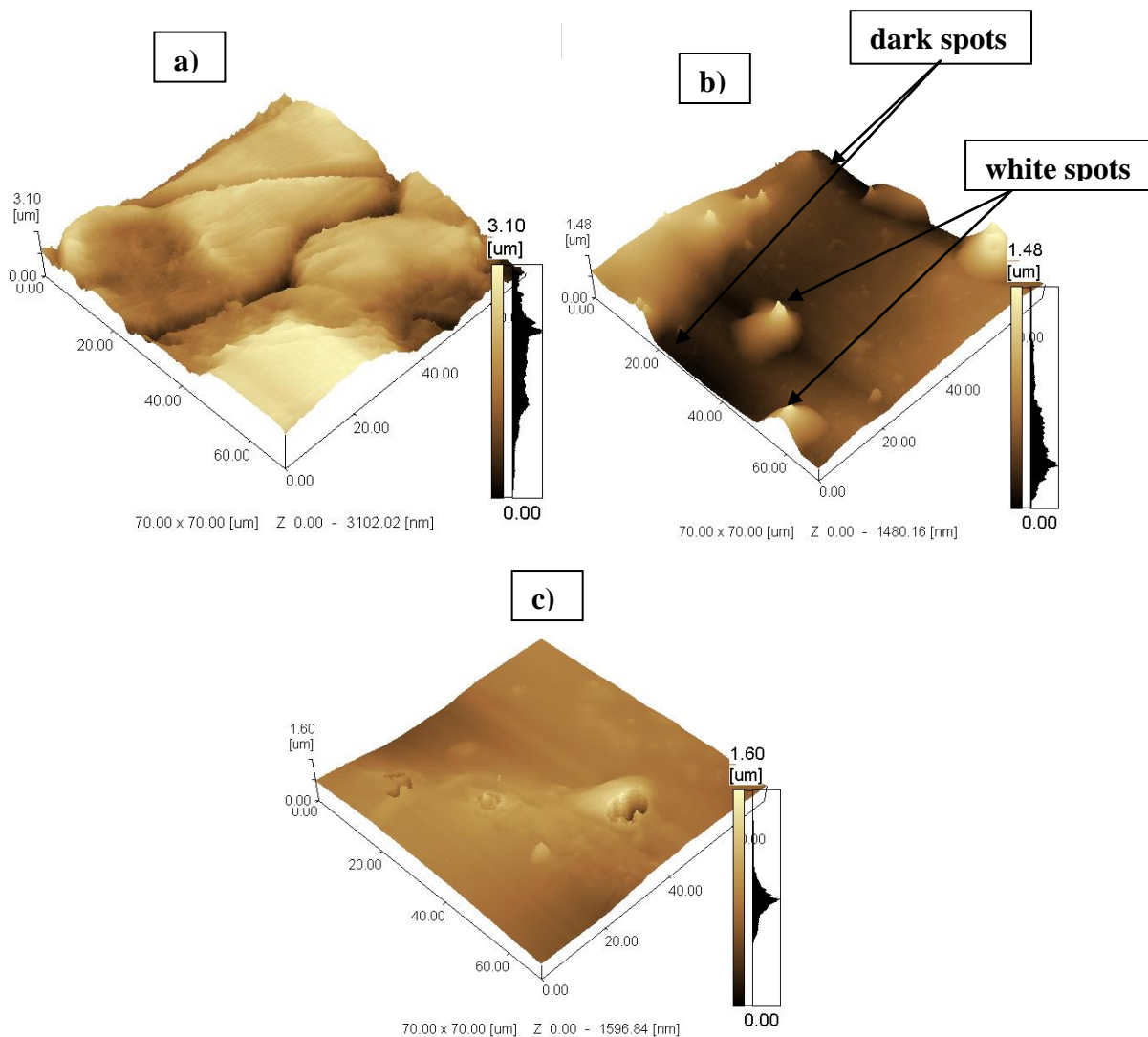


Figure 7. AFM height 3D to the samples: (a) HDG, (b) T0AN01 and (c) T4AN01.

Figure 7-a shows the bare galvanized steel, whose surface morphology is irregular, as expected. In Figure 7-b (T0AN01), some spots with higher heights can be observed, which are probably related to the formation of acrylate clusters (white spots). A dark spot can also be observed in the same image, which is related to the difference in the chemical composition in this particular region [41]. This may be associated with the T0AN01 sample containing a larger amount of MMA in the film, making it

irregular. During the curing process, non-polymerized MMA can volatilize, creating tensioned regions and leaving thinner films. This phenomenon can be observed in the lower layer thickness and the creation of defective areas. Still, it is possible to observe that the hybrid films possessed decreased roughness values compared to uncoated galvanized steel (Figure 7-a, Table 4), which means that both films (T0AN01 and T4AN01) covered the entire metal surface. Moreover, the morphology of the surface for T4AN01 is very smooth and flat with a very low roughness. The T4AN01 image (Figure 7-c) shows that this film entirely covers the surface.

Table 4. Roughness values for the studied samples.

Samples	AFM roughness		
	Ra (μm)	Rms (μm)	Peak to peak (μm)
HDG	4.99 ± 0.5	5.97 ± 0.6	5.64 ± 4.3
T0AN01	0.88 ± 0.7	1.15 ± 0.9	4.46 ± 3.1
T4AN01	0.17 ± 0.1	0.13 ± 0.1	1.09 ± 0.2

3.2. Physicochemical characterization

Figure 8 shows the images for the contact angle determination, and Table 5 shows the contact angles obtained for the uncoated galvanized steel and hybrid films (T0AN01 and T4AN01). The silane films exhibit hydrophobic character when sufficiently cross-linked. The contact angle of a well cross-linked film is approximately 90° [42]. It can be seen that the T0AN01 sample (Figure 8-b), without TEOS, showed the highest value for the contact angle, and consequently the lowest wettability. However, the T4AN01 sample (Figure 8-c) showed a decreased contact angle compared to the uncoated galvanized steel (Figure 8-a), which indicates that the addition of TEOS to the film did not reduce the wettability of the surface.

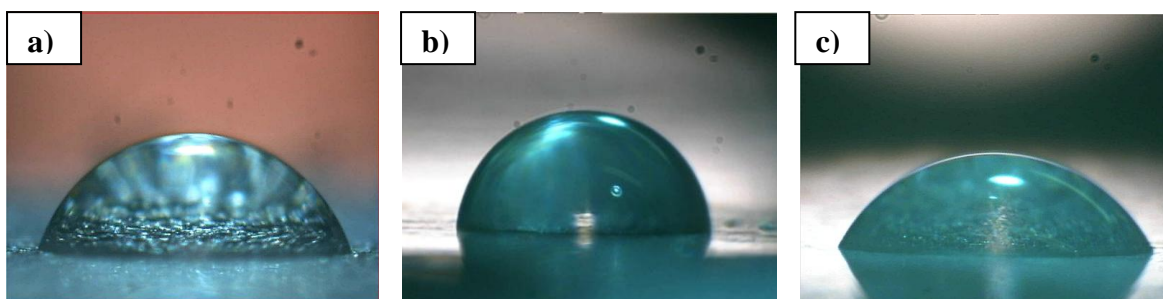


Figure 8. Images obtained for the contact angle determination by the sessile drop method: (a) HDG, (b) T0AN01 and (c) T4AN01.

This can be attributed to the characteristics of the precursors, in this case, to the hydrophilic character of TEOS. This film also presented a more accentuated formation of cracks, as verified by SEM (Figure 8-b). During the curing process, hydrophobic siloxane bonds are formed in the film network, which hinder water penetration. However, neither the precursor's hydrolysis nor cross-

linking (polycondensation) during curing is complete. Thus, non-hydrolyzed ester and hydrophilic OH groups are present. These ester and OH groups favor water uptake, while the siloxane groups can be hydrolyzed when the films are exposed to the electrolyte, further increasing the number of hydrophilic OH groups in the film.

Table 5. Contact angle values obtained by the sessile drop method.

Samples	Average contact angle
HDG	70 ± 0.74
T0AN01	87 ± 0.35
T4AN01	62 ± 0.61

Figure 9 and Table 6 show the IR spectra of the hybrid films. An intense band at 911 cm^{-1} is observed, related to the Si–O stretching of Si–OH groups that were not hydrolyzed. This peak is more intense for the siloxane-PMMA with TEOS (T4AN01), indicating less hydrolysis and subsequently less cross-linking of this sample. This indicates that neither the precursor's hydrolysis nor the cross-linking (polycondensation) is completed during the curing. Thus, non-hydrolyzed esters and hydrophilic OH groups are present in the films. This result is in agreement with the contact angle analysis (Table 5).

Approximately 1172 cm^{-1} , there is a strong band corresponding to the stretching of Si–O–Si bonds, which were formed by cross-linking during the curing process. The formation of a Si–O–Si layer results in a protective effect on the galvanized steel substrate. The bands close to 1728 and 1622 cm^{-1} are associated with the stretching vibrations of C=O and C=C groups. The bands at 1448 and 1387 cm^{-1} are attributed to the deformation vibrations of C–H bonds in the CH₂ and CH₃ groups. Finally, the band at 823 cm^{-1} is assigned to the C=C vibrations of the C=C–C=O group [43].

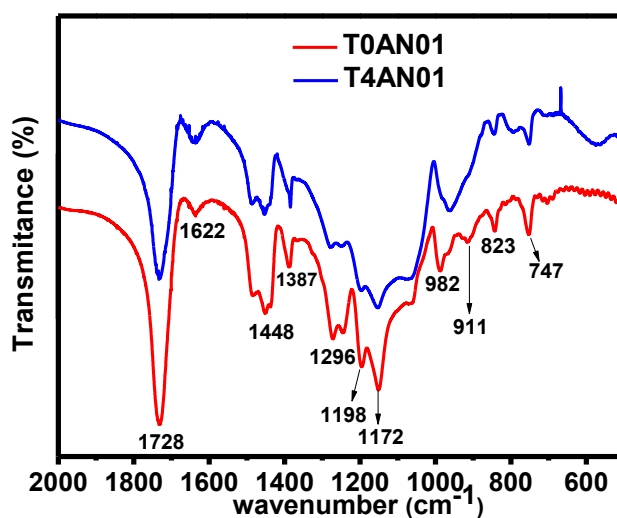


Figure 9. FI-IR spectra of the hybrid films: T0AN01 and T4AN01.

Table 6. FT-IR, peaks assignment as function of peak position.

Peak position (cm ⁻¹)	Peak assignment
700-800	C-H (Si-CH ₂ - CH ₂ -Si) stretch
800-880	C=C-C=O symmetric and asymmetric stretch
890-920	Si-O (Si-OH) stretch
900-990	Asymmetrical stretching Si-O-C ₂ H ₅ groups unhydrolyzed
1000-1250	Si-O stretching of Si-O-Si crosslinked
1300-1500	CH ₂ and CH ₃ scissoring
1600-1670	C=C-H axial deformation
1700-1750	C=O axial deformation

3.3. Electrochemical characterization

3.3.1. Open circuit potential

Open circuit potential (OCP) measurements of the samples were made versus time in 0.05 M NaCl, as illustrated in Figure 10. According to the OCP values for the samples covered with the hybrid films (T0AN01 and T4AN01), the potentials were less active than for uncoated galvanized steel (HDG). This means that the hybrid films promoted the formation of a barrier between the substrate and the solution. Previous results reported in the literature show that hybrid films confer a higher anti-corrosion resistance than silane films [44, 45]. However, it was not possible to observe a significant difference between the two samples in the open circuit potentials.

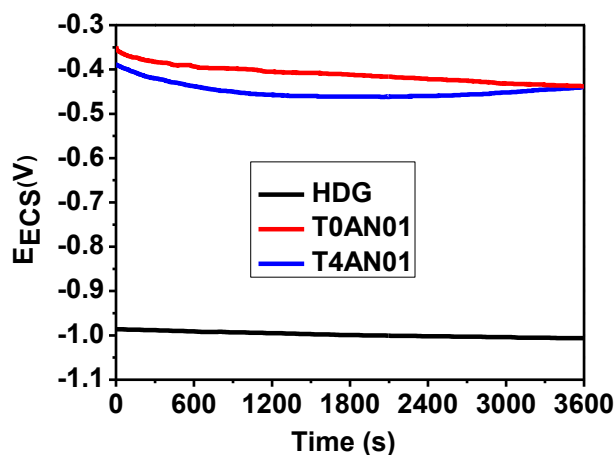


Figure 10. Open circuit potential curves for galvanized steel without coating (HDG) and coated with the films (T0AN01 and T4AN01).

3.3.2. Electrochemical impedance spectroscopy

Figure 11 and Figure 12 show the electrochemical impedance Bode diagrams for hybrid siloxane-PMMA films without TEOS (T0AN01) and with TEOS (T4AN01), respectively, as a

function of immersion time (24, 48, 72 and 96 h) in a 0.05 M NaCl solution. These diagrams were obtained sequentially for the same sample, and thus represent the evolution of the electrode response as a function of immersion time.

Electrical equivalent circuit models were used to fit the impedance curves. Tables **Error! Reference source not found.**7–9 show the electrical elements values obtained by fitting the hybrid siloxane-PMMA films (T0AN01 and T4AN01) and the uncoated galvanized steel up to 96 hours of immersion in 0.05 M NaCl. However, it was not possible to fit the impedance curves for the first hour of immersion due to their instability in the solution. In several circuits, the capacitance was substituted by a CPE to take into account the non-ideality of the hybrid films. A value of $n=1$ corresponds to a smooth surface; therefore, in this case, the CPE should be substituted by an ideal capacitor C . On the other hand, R_e is the electrolyte resistance, and RDF and CPEDF represent high to medium frequency elements associated with the resistance of hybrid siloxane-PMMA films. RPE and CPEPE represent medium to low frequency elements, which were attributed to the permeability resistance of the electrolyte through the defects of the hybrid film. RPC and CPEPC represent low frequency phenomena associated with the corrosion process.

A phenomenon of high to medium frequency can be observed in Figure 11 after only a 24-hour immersion, which was attributed to the resistance of the hybrid siloxane-PMMA film without TEOS (T0AN01). The fitting results showed an abrupt decrease of the RDF value after 24 hours (Table 7), and at the same time, diffusive pathways were established through the coating. This could be explained by the T0AN01 film structure, where the MMA radicals covalently bonded to the TMSM moieties through polymerization reactions can only interact by weak Van der Waals forces. Taking into account these structural considerations, a lower film thickness is expected, due to the weak bonding (Figure 6 and Table 3). Consequently, there is less resistance to long periods of immersion in 0.05 M NaCl.

After 48 and 72 hours of immersion, a third time constant was identified (Table **Error! Reference source not found.**7). A phenomenon of high to medium frequency with lower phase angle (Figure **Figure**11-a) was associated with the resistance of the electrolyte permeation through the defects of the siloxane-PMMA film without TEOS (T0AN01). A phenomenon of middle to low frequency was associated with the charge transfer reaction at the metal surface at the bottom of the silane coating pores [46], as observed in the SEM images (Figure 4) where there are small cracks in the film. These cracks constitute the conductive pathways that can be widened upon exposure to the electrolyte, promoting easier access of aggressive species to the substrate surface; this explains the decrease in both the pore and diffusion resistance [47]. Finally, a low frequency phenomenon associated with the corrosion process was identified.

After 96 h, only two time constants were identified (Table 7), indicating that the coating was no longer detected by the EIS measurement. A phenomenon of high to medium frequency with lower phase angle (Figure 11-a) was attributed to the resistance of the permeability of the electrolyte through the defects of the siloxane-PMMA film without TEOS (T0AN01). A phenomenon of middle to low frequency was associated with the charge transfer reaction at the metal surface at the bottom of the silane coating pores. For this situation, the resistance (RPE) associated with the charge transfer process was even lower than in the previous experiments, and the electrode surface presented visible signs of corrosion with the formation of a red precipitate.

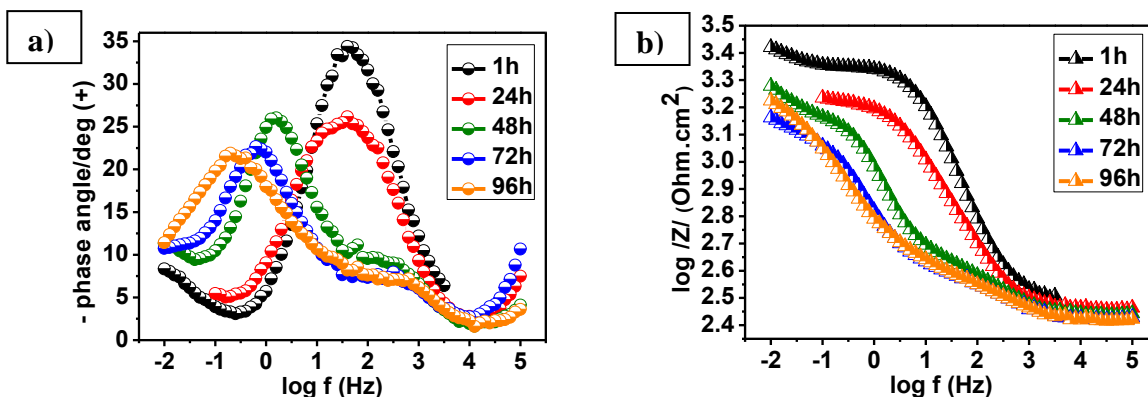


Figure 11. EIS Bode phase angle (a) and modulus (b) plots obtained as a function of exposure time in 0.05M NaCl solution to the sample T0AN01.

Table 7. Electrical elements fitted values for T0AN01 film up to 96 h of immersion in a 0.05M NaCl solution.

T0AN01	24h	48h	72h	96h
Fitted circuit				
Re ($\Omega.cm^2$)	169.7	168.1	158.3	143.1
CPEDF (Fcm^{-2})	9.46×10^{-05}	1.10×10^{-04}	2.2×10^{-04}	7.14×10^{-04}
N	0.62	0.65	0.55	0.38
RDF ($\Omega.cm^2$)	950.9	138.5	119.3	204.4
CPEPE(Fcm^{-2})		3.37×10^{-04}	8.40×10^{-04}	1.10×10^{-03}
N		0.83	0.76	0.66
RPE ($\Omega.cm^2$)		675.5	582.1	456
CPEPC (Fcm^{-2})		2.73×10^{-02}	3.90×10^{-02}	
N		0.89	0.72	
RPC($\Omega.cm^2$)		455.9	890.6	

In Figure 12, it was observed that over the period of immersion (24, 48, 72 and 96 h), three time constants (Table 8) could be used to fit the EIS data, which encompass a diffusive element. A phenomenon of high to medium frequency (Figure 9-a) was associated with the resistance of the hybrid siloxane-PMMA film with TEOS (T4AN01). A phenomenon of middle to low frequency was attributed to the charge transfer reaction at the metal surface at the bottom of the silane coating cracks, as observed in the SEM images (Figure 5) where accentuated crack formation was observed. The results showed a significant decrease of RDF with time, indicating easier penetration of the electrolyte. Finally, in the phenomenon of low frequency, the corrosion process was detected with a time constant associated with RPC in parallel with CPEPC. After a 24-hour immersion, the values related to the diffusion resistance continuously decreased, indicating that electrochemically active species more easily reach the electrode surface. Accordingly, the charge transfer resistance also decreased, pointing to faster interfacial electrochemical processes [48].

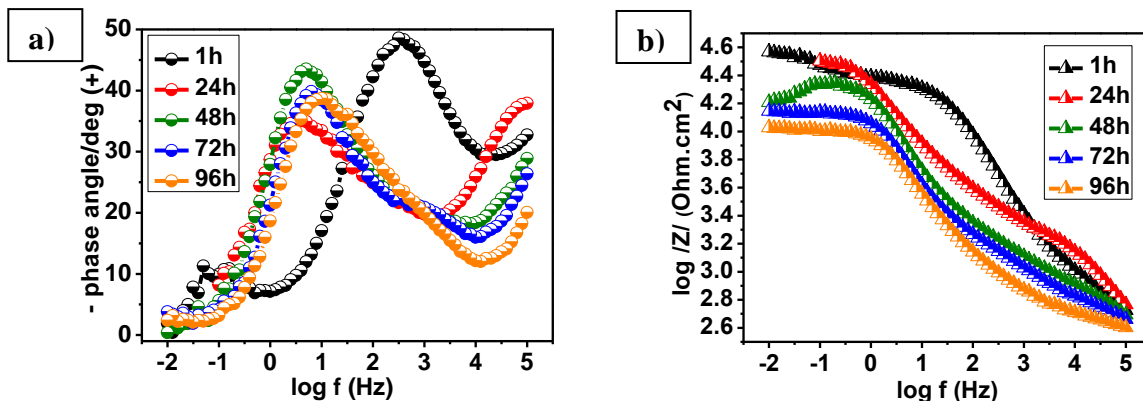


Figure 12. EIS Bode phase angle (a) and modulus (b) plots obtained as a function of exposure time in 0.05M NaCl solution for the sample T4AN01.

Table 8. Electrical elements fitted values for T4AN01 film up to 96 h of immersion in a 0.05M NaCl solution.

T4AN01	24h	48h	72h	96h
Fitted circuit				
Re (Ω.cm²)	68.63	63.0	63.0	65.0
CPEDF (Fcm⁻²)	5.73 x 10 ⁻⁰⁷	7.78 x 10 ⁻⁰⁷	4.99 x 10 ⁻⁰⁷	6.14 x 10 ⁻⁰⁷
n	0.64	0.61	0.64	0.64
RDF (Ω.cm²)	1133	539.1	384.0	282.5
CPEPE(Fcm⁻²)	7.32 x 10 ⁻⁰⁶	6.77 x 10 ⁻⁰⁶	7.84 x 10 ⁻⁰⁶	8.95 x 10 ⁻⁰⁶
n	0.65	0.67	0.66	0.71
RPE (Ω.cm²)	3644	1342	1072	830.7
CPEPC (Fcm⁻²)	1.01 x 10 ⁻⁰⁵	8.65 x 10 ⁻⁰⁶	1.14 x 10 ⁻⁰⁵	1.29 x 10 ⁻⁰⁵
n	0.72	0.81	0.82	0.77
RPC(Ω.cm²)	19521	14552	8059	5791

Figure 13 and Figure 14 show the evolution of the coating properties (i.e., the resistance and capacitance, respectively) as a function of immersion time. Generally, the high frequency resistance values (Figure 13) decreased during the first hours of immersion, due to the development of conductive pathways inside the film [49]. The T4AN01 sample exhibited the highest resistance at all times (Figure 13); this is due to the larger layer thicknesses obtained for this system (Figure 6 and Table 3) compared to the T0AN01 sample. Moreover, this demonstrates the excellent synergistic effect of covalent TEOS/TMSM.

The evolution of the coating resistance is a major characteristic of the barrier properties of a protective layer [50]. Both systems showed a sharp reduction of the resistance values from 24 hours to 48 hours of immersion, the T0AN01 sample more sharply. Subsequently, the resistance of the T4AN01 coating decreases slowly over an immersion time of 96 hours, which reflects the stability of the coating and its good barrier properties [51]. In contrast, the coating without TEOS (T0AN01) loses its barrier

properties after 48 hours of immersion. This rapid decrease is related to the formation of new defects and pores in the coatings.

In Figure 14, it is observed that the T4AN01 sample had capacitance values three orders of magnitude smaller than the T0AN01 sample, highlighting the improved performance properties of the hybrid film barriers with TEOS. Furthermore, there is an increase in the capacitance of the T0AN01 coating after 48 hours of immersion, which can be explained by a reduction in the coating thickness and/or conductivity, and therefore an increase in the porosity [52].

A slight increase in the capacitance is observed in the T4AN01 sample (Figure 14) after the 48 hour immersion, which is associated with the absorption of electrolyte. After 96 hours of immersion, another small but significant increase in the capacitance of the film was observed, as a result of water absorption, which occurred due to the reduced barrier properties of the film [52].

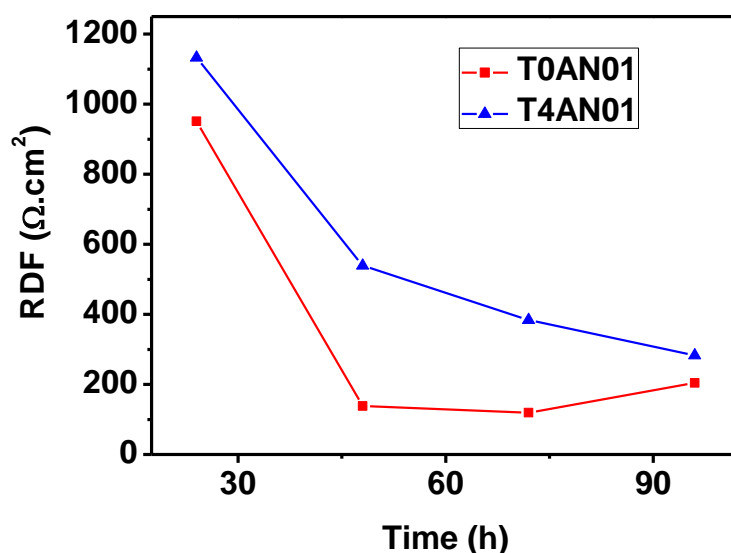


Figure 13. Evolution of the hybrid films resistance for T0AN01 and T4AN01 in a 0.05M NaCl solution with the immersion time.

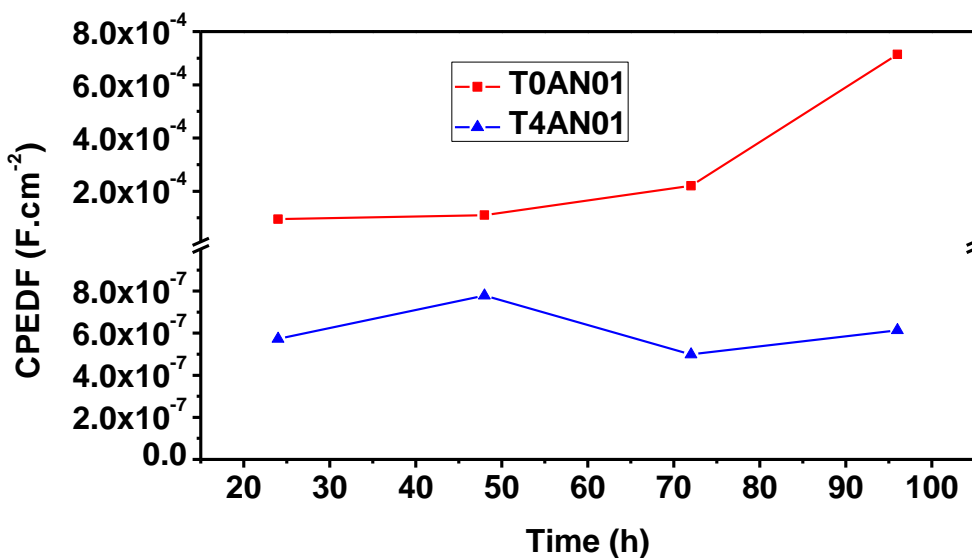
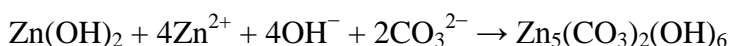


Figure 14. Evolution of the hybrid films constant phase element for T0AN01 and T4AN01 in a 0.05M NaCl solution with the immersion time.

For the uncoated galvanized steel (Figure 15 and Table 9), two time constants were observed over the entire immersion time (1, 24, 48, 72, and 96 h). The phenomenon at low frequency may be related to the diffusion limitations caused by the high reaction rate. The response of the charge transfer becomes shifted to lower frequencies as the active area expands, increasing the capacitance. Meanwhile, another process with very low resistance appears at the medium frequency, which may result from the cathodic reaction or from the precipitation of zinc hydroxide as shown below [53].



According to the Pourbaix diagram for zinc, zinc hydroxide is stable at pH values above 8, a value that is easily reached over steel. Further, carbonates can also form, eventually leading to hydrozincite as shown below [54].



The majority of the publications applying impedance to corroding systems use continuous metals and not galvanic couples. In such a system, the interpretation of the impedance spectra may be facilitated by the results for the separate metals. In this case, is interesting to note that the HDG showed lower values of resistance and higher values of capacitance (Table 9) compared to the hybrid films (Table 7 and Table 8) and lower impedance modulus and phase angle (Figure 15) relative to the hybrid films studied (T0AN01 and T4AN01) at all immersion times analyzed.

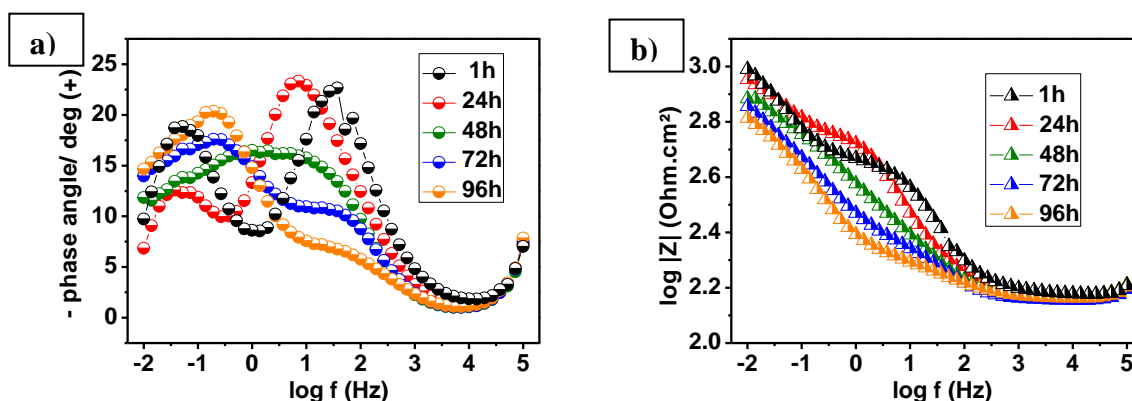
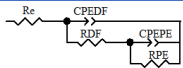
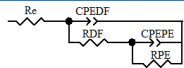
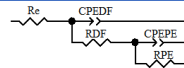
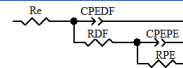
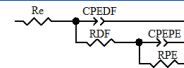


Figure 15. EIS Bode phase angle (a) and modulus (b) plots obtained as a function of exposure time in 0.05M NaCl solution for the sample HDG.

The SEM micrographs for the siloxane-PMMA samples (T0AN01 and T4AN01) after the electrochemical impedance test are shown in Figure 16. As can be observed, the T4AN01 sample (Figure 16-b) showed a lower attack of the formed film, demonstrating the superior performance of this coating, as already discussed. The T0AN01 sample (Figure 16-a) and HDG (Figure 16-c) were completely destroyed by the chloride solution.

Table 9. Electrical elements fitted values for HDG up to 96 h of immersion in a 0.05M NaCl solution.

HDG	1h	24h	48h	72h	96h
Fitted circuit					
Re (Ω.cm²)	151	150,8	148,5	151,3	146,9
CPEmf (Fcm⁻²s)	1,0 x 10 ⁻⁶	1.08 x 10 ⁻⁴	2,80 x 10 ⁻⁴	2,41 x 10 ⁻⁴	2,29 x 10 ⁻⁴
n	0,75	0,74	0,66	0,90	0,80
Rmf (Ω.cm²)	466	468	252,2	192,3	178,29
CPEbf (Fcm⁻²)	6,53 x 10 ⁻³	6.5 x 10 ⁻³	14,6 x 10 ⁻³	1,6 x 10 ⁻³	3,67 x 10 ⁻³
n	0,82	0,81	0,90	0,30	0,55
Rbf(Ω.cm²)	1085	1155	956,2	1231,0	866,79

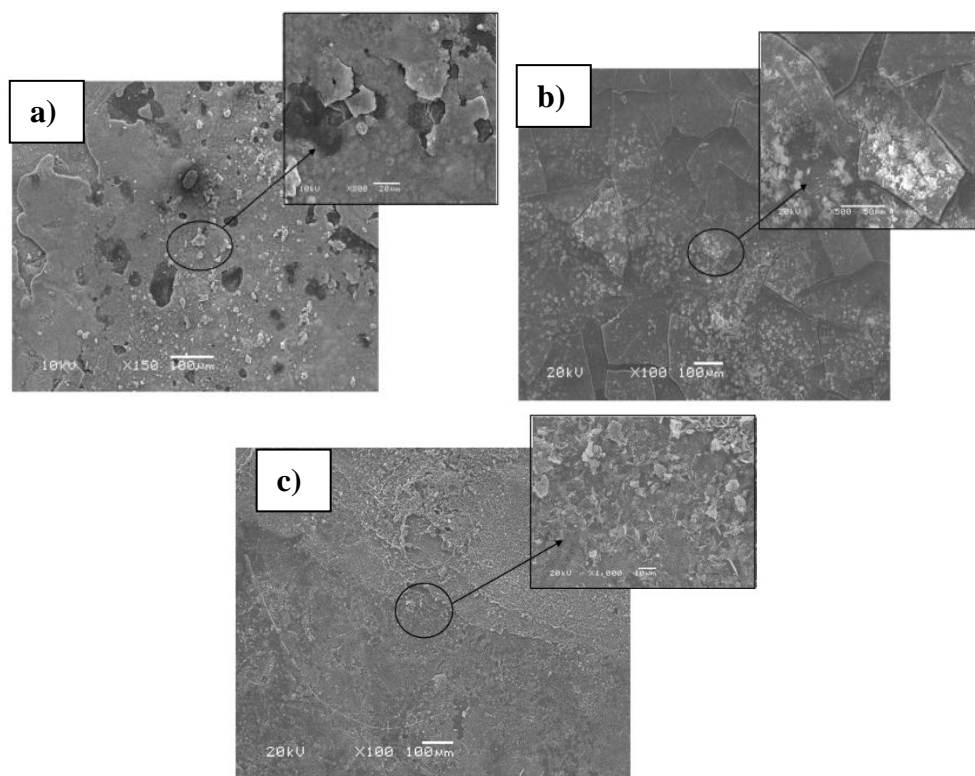


Figure 16. SEM micrographs obtained after 96 hours of testing electrochemical impedance for the samples: (a) T0AN01, (b) T4AN01 and (c) HDG.

3.4 Mechanical characterization

Figure 17 shows the coefficient of friction (COF) with the sliding time for the studied hybrid films. It can be observed that the addition of TEOS to the siloxane-PMMA hybrid film resulted in a higher durability in the film wear test. This high value is associated with the higher layer thickness and the synergistic effect of the covalent TEOS/TMSM system.

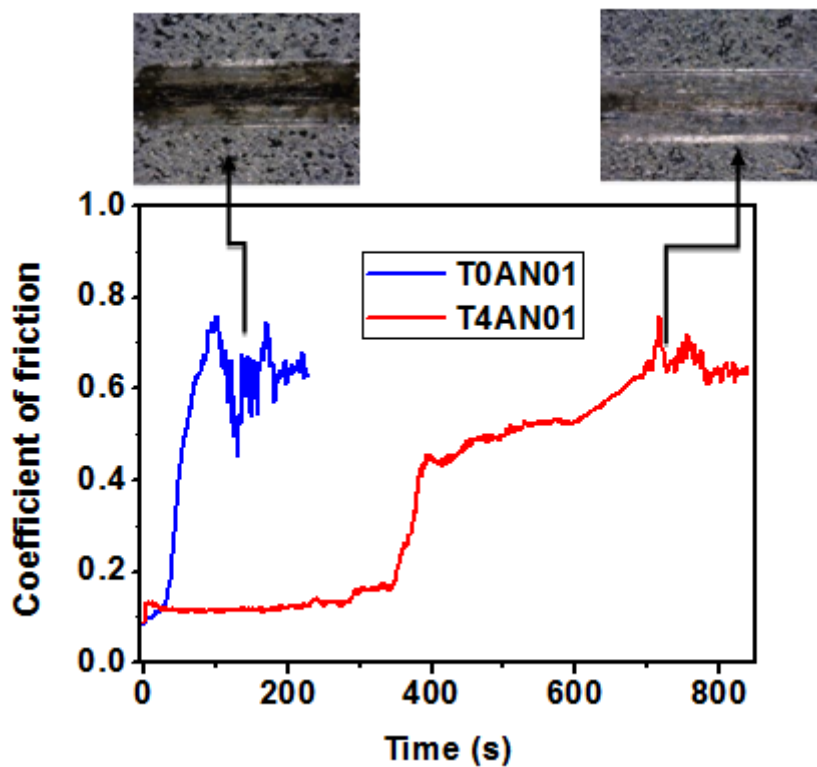


Figure 17. Friction coefficients of the hybrid films T0AN01 and T4AN01.

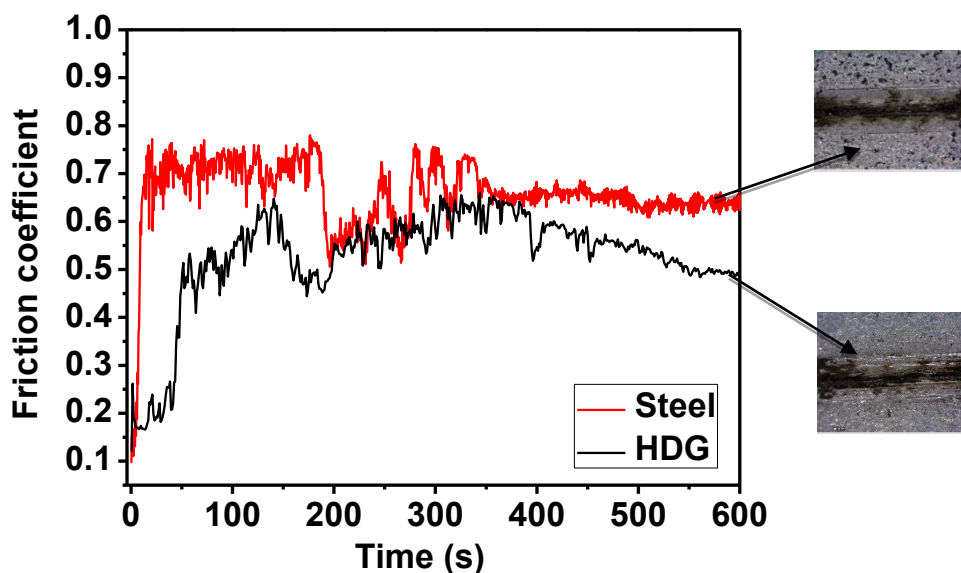


Figure 18. Friction coefficients of the galvanized steel without coating and steel.

Moreover, it is noted that the sample without TEOS (T0AN01) had wear resistance values that are very similar to those of the uncoated galvanized steel (Figure 18), denoting high hardness and low brittleness wear resistance. This coating is very similar to zinc [55], as seen in the optical images. This could be explained by the T0AN01 film structure, where the radical of MMA covalently bonds to the

TMSM moieties through polymerization reactions and can only interact by weak Van der Waals forces. Taking into account these structural considerations, a lower thickness of the film is expected due to the weak bonding; this results in a poor performance in the wear test. The change in the coefficient of friction seen in Figure 18 determines the exchange of the tribological pair, i.e., the ruptured film. As seen in Figure 18, the coefficients of friction of the hybrid film samples reached a stable level ($\mu=0.7$) after the breakup of the films. This indicates that the films had a high adherence to Zn such that upon breaking, the hybrid film also breaks off of Zn.

4. CONCLUSIONS

The results obtained showed that the hybrid siloxane-PMMA films presented a regular and even covering on the galvanized steel. However, these films presented cracks, thus compromising the corrosion resistance of the T0AN01 sample, which possessed a lower thickness compared to the T4AN01 sample with added TEOS, indicating the effective barrier effect of this latter film. Still, it was possible to observe the shift in the open circuit potential of the galvanized steel towards less active values after the application of the hybrid films. The EIS results and mechanical characterization showed that the T4AN01 coating presented the best performance.

The results obtained for the T4AN01 film showed a higher film thickness, attributed to the presence of TEOS in the film, which increases the silanol content and consequently increases the amount of inorganic phase (siloxane). It was also observed that the higher thickness of this film was partly due to the covalent bonds of the organic and inorganic precursors. This demonstrates the synergistic effect of the combination of the TMSM and TEOS precursors.

ACKNOWLEDGMENTS

The authors would like to express their gratitude for the financial support of CAPES (the Brazilian Government agency for the development of human resources), CNPq (the Brazilian National Council for Scientific and Technological Development) and PRONEX/FAPITEC (Excellence Program by Foundation for Research Support and Innovation in the State of Sergipe)

References

1. W. Trabelsi, L. Dhouibi, E. Triki, M.G.S. Ferreira and M.F. Montemor, *Surf. Coat. Technol.*, 192 (2005) 284.
2. J. Kasperek, D. Verchere, D. Jacquet and N. Phillips, *Mater. Chem. Phys.*, 56 (1998) 205.
3. S. Dalbin, G. Maurin, R.P. Nogueira, J. Persell and N. Pommier, *Surf. Coat. Technol.*, 194 (2005) 363.
4. R. Romero-Pareja, R. López-Ibáñez, F. Martín, J.R. Ramos-Barrado and D. Leinen, *Surf. Coat. Technol.*, 200 (2006) 6606.
5. Y.K. Song and F. Mansfeld, *Corros. Sci.*, 48 (2006) 154.
6. A.N. Khramov, V.N. Balbyshev, N.N. Voevodin and M.S. Donley, *Prog. Org. Coat.*, 47 (2003) 207.
7. A.V. Cunliffe, S. Evans, D.A. Tod, S.A. Torry and P. Wylie, *Int. J. Adhes. Adhes.*, 21 (2001) 287.
8. B. Chico, J.C. Galván and D. de la Fuente, *Prog. Org. Coat.*, 60 (2007) 45.

9. B.L. Lin, J.T. Lu, G. Kong and J. Liu, *Surf. Coat. Technol.*, 17 (2007) 755.
10. F. Zucchi, V. Grassi, A. Frignani and G. Trabanelli, *Corros. Sci.* 46 (2004) 2853.
11. F. Zucchi, A. Frignani, V. Grassi, G. Trabanelli and M. DalColle, *Corros. Sci.*, 49 (2007) 1570.
12. J. Kim, K.C. Wong, P.C. Wong, S.A. Kulinich and J.B. Metson, *Appl. Surf. Sci.*, 253 (2007) 4197.
13. W. Trabelsi, P. Cecilio, M.G.S. Ferreira, K. Yasakau, M.L. Zheludkevich and M.F. Montemor, *Prog. Org. Coat.*, 59 (2007) 214.
14. M.F. Montemor and M.G.S. Ferreira, *Electrochim. Acta*, 52 (2007) 6976.
15. U. Schubert, N. Huesing and A. Lorenz, *Chem. Mater.*, 7 (1995) 2010.
16. C. Sanchez and F. Ribbot, *New J. Chem.*, 18 (1994) 1007.
17. J. Wen and G.L. Wilkes, *Chem. Mater.*, 8 (1996) 1667.
18. P. Judeinstein and C. Sanchez, *J. Mater. Chem.*, 6 (1996) 511.
19. G. Schottner, *Chem. Mater.*, 13 (2001) 3422.
20. M.F. Ashby and Y.J.M. Bréchet, *Acta Mater.*, 51 (2003) 5801.
21. G. Schulz-Ekloff, D. Wöhrle, B. van Duffel and R.A. Schoonheydt, *Microporous Mesoporous Mater.*, 51 (2002) 91.
22. K. Iketani, R.D. Sun, M. Toki, K. Hirota and O. Yamaguchi, *J. Phys. Chem. Solids*, 64 (2003) 507.
23. M.D. Rahn and T.A. King, *Appl. Opt.*, 34 (1995) 8260.
24. P.F.W. Simon, R. Ulrich, H.W. Spiess and Ulrich Wiesner, *Chem. Mater.*, 13 (2001) 3464.
25. P. Proposito, M. Casalbani, F. De Matteis, M. Glasbeek, A. Quatela, E. Van Veldhoven and H. Zhang, *J. Lumin.* 94–95 (2001) 641.
26. I.G. Marino, D. Bersani and P.P. Lottici, *Opt. Mater.*, 15 (2001) 279.
27. K.C. Song, J.K. Park, H.U. Kang and S.H. Kim, *J. Sol-Gel Sci. Technol.*, 27 (2003) 53.
28. H. Hirashima, H. Imai and Y. Fukui, *J. Sol-Gel Sci. Technol.*, 26 (2003) 383.
29. G. Gu, Z. Zhang and H. Dang, *Appl. Surf. Sci.*, 221 (2004) 129.
30. D. Cangialosi, P. T. Mcgrail, G. Emmerson, A. Valenza, E. Calderaro and G. Spadaro, *Nucl. Instrum. Methods Phys. Res., Sect. B*, 185 (2001) 262.
31. Y. T. Shieh, K. H. Liu and T. L. Lin, *J. Supercrit. Fluids*, 28 (2004) 101.
32. S. Gu, T. Kondo and M. Konno, *J. Colloid Interface Sci.*, 272 (2004) 314.
33. J. Luna-Xavier, A. Guyot and E. Bourgeat-Lami, *J. Colloid Interface Sci.*, 250 (2002) 82.
34. H. Sertchook and D. Avnir, *Chem. Mater.*, 15 (2003) 1690.
35. J. U. Park, W. S. Kim and B. S. Bae, *J. Mater. Chem.*, 13 (2003) 738.
36. A. Zhu, Z. Shi, A. Cai, F. Zhao and T. Liao, *Polym. Test.*, 27 (2008) 540.
37. N. Katsikis, F. Zahradnik, A. Helmschrott, H. Munstedt and A. Vital, *Polym. Degrad. Stab.*, 92 (2007) 1966.
38. L. Delattre, C. Dupuy and F. Babonneau, *J. Sol-Gel Sci. Technol.*, 2 (1994) 185.
39. X. Zhang, Y. Wu, S. He and D. Yang, *Surf. Coat. Technol.*, 201 (2007) 6051.
40. S. Zaioncz, K. Dahmouche, C.M. Paranhos, R.S.S. Gil and B.G. Soares, *Express Polym. Lett.*, 3 (2009) 340.
41. S.N. Magonov, V. Elings and M.H. Whangbo, *Surf. Sci.*, 375 (1997) L385.
42. W.J. van Ooij, D. Zhu, M. Stacy, A. Seth, T. Mugada, J. Gandhi and P. Puomi, *Tsinghua Science and Technology*, 10 (2005) 639.
43. M. Pantoja, B. Díaz-Benito, F. Velasco, J. Abenojar and J.C. del Real, *Appl. Surf. Sci.*, 255 (2009) 6386.
44. M. Behzadnasab, S.M. Mirabedini, K. Kabiri and S. Jamali, *Corros. Sci.*, 53 (2011) 89.
45. P. Hammer, M.G. Schiavetto, F.C. Dos Santos, A.V. Benedetti, S.H. Pulcinelli and C.V. Santilli, *J. Non-Cryst. Solids*, 356 (2010) 2606.
46. B. Chico, J.C. Galván, D. De La Fuente and M. Morcillo, *Prog. Org. Coat.*, 60 (2007) 45.
47. R.G. Duarte, A.S. Castela and M.G.S. Ferreira, *Prog. Org. Coat.*, 57 (2006) 408.
48. B. Hirschorn, M.E. Orazem, B. Tribollet, V. Vivier, I. Frateur and M. Musiani, *Electrochim. Acta*, 55 (2010) 6218.

49. M.F. Montemor, R. Pinto and M.G.S. Ferreira, *Electrochim. Acta*, 54 (2009) 5179.
50. M. Schem, T. Schmidt, J. Gerwann, M. Wittmar, M. Veith, G.E. Thompson, I.S. Molchan, T. Hashimoto, P. Skeldon, A.R. Phani, S. Santucci and M.L. Zheludkevich, *Corros. Sci.*, 51 (2009) 2304.
51. Roohangiz Zandi Zand, Kim Verbeken and Annemie Adriaens, *Int. J. Electrochem. Sci.*, 8 (2013) 548.
52. C. Motte, M. Poelman, A. Roobroeck, M. Fedel, F. Deflorian and M.G. Olivier, *Prog. Org. Coat.*, 74 (2012) 326.
53. A.M. Simões and J.C.S. Fernandes, *Prog. Org. Coat.*, 69 (2010) 219.
54. K. Ogle, S. Morel and J. Jacquet, *J. Electrochem. Soc.*, 153 (2006) B1–B5.
55. Chai Zhimin, Lu Xinchun and He Dannong, *Surf. Coat. Technol.*, 207 (2012) 361.